Studies of piezooptic coefficients in $LiNbO_3$ crystals using a crystalline disk compressed along its diameter

Vasylkiv Yu., Savaryn V., Smaga I., Krupych O., Skab I. and Vlokh R.

Institute of Physical Optics, 23 Dragomanov St., 79005 Lviv, Ukraine,
e-mail: vlokh@ifo.lviv.ua

Received: 02.11.2011

Abstract. We have suggested a highly precise method for determining piezooptic coefficients, which relies on a knowledge of 2D spatial distribution of mechanical stresses in a crystalline disk compressed along its diameter. Relevant theoretical relations that describe piezooptic effect in the crystals belonging to the point symmetry group 3m have been derived. The method has been successfully verified in the experiment dealing with $LiNbO_3$ crystals.

Keywords: piezooptic effect, 2D distribution of mechanical stresses, crystalline disks, lithium niobate

PACS: 78.20.H-, 78.20.Ci, 07.10.Lw
UDC: 535.012

1. Introduction

Piezooptic effect represents a well-known optical phenomenon that consists in changes of refractive indices of an optical medium under the action of mechanical stresses [1]. Using tensorial description, one can present the relation between the increments of optical-frequency impermeability tensor ΔB_i and the mechanical stresses σ_l as

$$\Delta B_i = \Delta\left(\frac{1}{n^2}\right)_i = \pi_{il}\sigma_l , \qquad (1)$$

where π_{il} is the fourth-rank polar tensor of piezooptic coefficients and n the refractive index. Although the piezooptic effect has been discovered almost two centuries ago [2, 3], the experimental methods for its study are still being improved. This is because the accuracy of determination of the piezooptic coefficients is often very low, especially for anisotropic low-symmetry crystals, while the experimental errors can reach 30% or even larger values (see, e.g., [4]).

As we have earlier shown [4], these errors are caused by inhomogeneous spatial distribution of mechanical stresses inside a sample appearing under its uniaxial loading, due to a friction force that arises between the sample surfaces and the substrates, and a barrel-shaped deformation of that sample. It has been found that all the six components of a symmetric second-rank stress tensor arise under such an action, with their spatial distributions being unpredictable. As a result, the actual value of the mechanical stress, which induces changes in the refractive indices, is in fact unknown. The second source of the high errors follows from complicated theoretical relations among the optical phase retardations under measuring and the mechanical stresses, which usually involves a lot of piezooptic tensor components. Thus, when determining one of these components in practice, one should measure the others in some additional experiments (see, e.g., [5, 6]). This fact leads to additional increase in the piezooptic errors.

Let us consider this problem in a more detail. As shown in our recent work [4], the first problem consisting in appearance of inhomogeneous stresses inside a sample under its uniaxial

loading can be solved by creating two-dimensional (2D) inhomogeneous stresses in the sample, with in advance known distributions of the stress tensor components along the two transverse Cartesian coordinates. Notice that the optical retardation and the orientation of optical indicatrix should not depend upon the third longitudinal coordinate, along which the optical beam propagates. Hence, the errors for some of the piezooptic tensor components can be reduced down to 3–12% owing to application of torsion or bending stresses. It is known [7] that any torsion moment induces shear stresses, while bending leads to appearance of compression (or tension) stresses in samples. Considering the piezooptic tensor presented in its matrix form,

$$\begin{array}{c|ccc:ccc} & \sigma_1 & \sigma_2 & \sigma_3 & \sigma_4 & \sigma_5 & \sigma_6 \\ \hline \Delta B_1 & \pi_{11} & \pi_{12} & \pi_{13} & \pi_{14} & \pi_{15} & \pi_{16} \\ \Delta B_2 & \pi_{21} & \pi_{22} & \pi_{23} & \pi_{24} & \pi_{25} & \pi_{26} \\ \Delta B_3 & \pi_{31} & \pi_{32} & \pi_{33} & \pi_{34} & \pi_{35} & \pi_{36} \\ \hdashline \Delta B_4 & \pi_{41} & \pi_{42} & \pi_{43} & \pi_{44} & \pi_{45} & \pi_{46} \\ \Delta B_5 & \pi_{51} & \pi_{52} & \pi_{53} & \pi_{54} & \pi_{55} & \pi_{56} \\ \Delta B_6 & \pi_{61} & \pi_{62} & \pi_{63} & \pi_{64} & \pi_{65} & \pi_{66} \end{array}, \qquad (2)$$

one can see that all of the piezooptic tensor components can be involved into piezooptic interaction in consequence of application of bending or torsion stresses. For convenience, we divide the piezooptic tensor given by Eq. (2) into four parts. The first part (A) corresponds to the coefficients that describe compression (or expansion) of the optical indicatrix ellipsoid along its principal axes, as a result of compressive or tension stresses. The second one (B) describes the same changes in the optical indicatrix, though taking place under shear stresses. The coefficients of the third (C) and fourth (D) parts describe rotations of the optical indicatrix under normal and shear stresses, respectively. Our earlier works [8–11] have demonstrated that the coefficients appearing in the first and second parts of the piezooptic matrix can be determined with high enough accuracy using bending or torsion of samples, respectively. However, precise determination of the coefficients figuring in the third and fourth parts still represents a conspicuous problem.

The present work is devoted to further development of the methods for determination of piezooptic coefficients, in particular those belonging to the third and fourth parts of the matrix given by Eq. (2). Our method essentially relies on creating 2D stress distribution in a crystalline disk compressed along its diameter.

2. Relations for the optical indicatrix in case of crystalline disc compressed along its diameter

It is known [12] that, besides the torsion and bending, loading of a crystalline disk along its diameter can also create a 2D stressed state. When the disk is perpendicular to Z axis and the loading force P is applied along Y axis, the following three components of the stress tensor appear:

$$\sigma_1 = -\frac{2P}{\pi d}\left[\frac{(R-Y)X^2}{\left(X^2+(R-Y)^2\right)^2}+\frac{(R+Y)X^2}{\left(X^2+(R+Y)^2\right)^2}-\frac{1}{2R}\right], \qquad (3)$$

$$\sigma_2 = -\frac{2P}{\pi d}\left[\frac{(R-Y)^3}{\left(X^2+(R-Y)^2\right)^2}+\frac{(R+Y)^3}{\left(X^2+(R+Y)^2\right)^2}-\frac{1}{2R}\right], \qquad (4)$$

$$\sigma_6 = \frac{2P}{\pi d}\left[\frac{(R-Y)^2 X}{\left(X^2+(R-Y)^2\right)^2} - \frac{(R+Y)^2 X}{\left(X^2+(R+Y)^2\right)^2}\right], \tag{5}$$

with d being the thickness of the disk and R its radius. Let us consider the crystalline disk made of lithium niobate. The piezooptic tensor for the point group 3m, of which $LiNbO_3$ crystals are representatives, may be presented as

$$\pi_{il} = \begin{pmatrix} \pi_{11} & \pi_{12} & \pi_{13} & \pi_{14} & 0 & 0 \\ \pi_{12} & \pi_{11} & \pi_{13} & -\pi_{14} & 0 & 0 \\ \pi_{31} & \pi_{31} & \pi_{33} & 0 & 0 & 0 \\ \pi_{41} & -\pi_{41} & 0 & \pi_{44} & 0 & 0 \\ 0 & 0 & 0 & 0 & \pi_{44} & 2\pi_{41} \\ 0 & 0 & 0 & 0 & \pi_{14} & \pi_{66} \end{pmatrix}. \tag{6}$$

2.1. A disk perpendicular to Z axis

With accounting for the mechanical stress components involved in Eqs. (3)–(5) and the equality $\pi_{11} - \pi_{12} = \pi_{66}$ valid for the symmetry group 3m, one can get the following relation for the cross section of the optical indicatrix of $LiNbO_3$ by the plane $Z = 0$:

$$(B_{11} + \pi_{11}\sigma_1 + \pi_{12}\sigma_2)X^2 + (B_{11} + \pi_{12}\sigma_1 + \pi_{11}\sigma_2)Y^2 + 2(\pi_{11} - \pi_{12})\sigma_6 XY = 1. \tag{7}$$

The angle of the optical indicatrix rotation around the Z axis becomes

$$\tan 2\zeta_3 = \frac{2(\pi_{11} - \pi_{12})\sigma_6}{(B_1 + \pi_{11}\sigma_1 + \pi_{12}\sigma_2) - (B_1 + \pi_{12}\sigma_1 + \pi_{11}\sigma_2)} = \frac{2\sigma_6}{(\sigma_1 - \sigma_2)}. \tag{8}$$

Then the optical birefringence appearing for the case of light propagation along this axis is determined by

$$\Delta n_{12} = -\frac{1}{2} n_o^3 (\pi_{11} - \pi_{12})\sqrt{(\sigma_1 - \sigma_2)^2 + 4\sigma_6^2}. \tag{9}$$

The spatial distributions of the birefringence and the angle of optical indicatrix rotation simulated for the XY plane of the $LiNbO_3$ crystals are presented in Fig. 1. Here we have put $P = 100$ N, $d = 2$ mm, $R = 10$ mm and $\pi_{11} - \pi_{12} = -0.47 \times 10^{-12}\,\mathrm{m^2/N}$, while $n_o = 2.287$ and $n_e = 2.203$ are respectively the ordinary and extraordinary refractive indices at $\lambda = 632.8$ nm [13, 14].

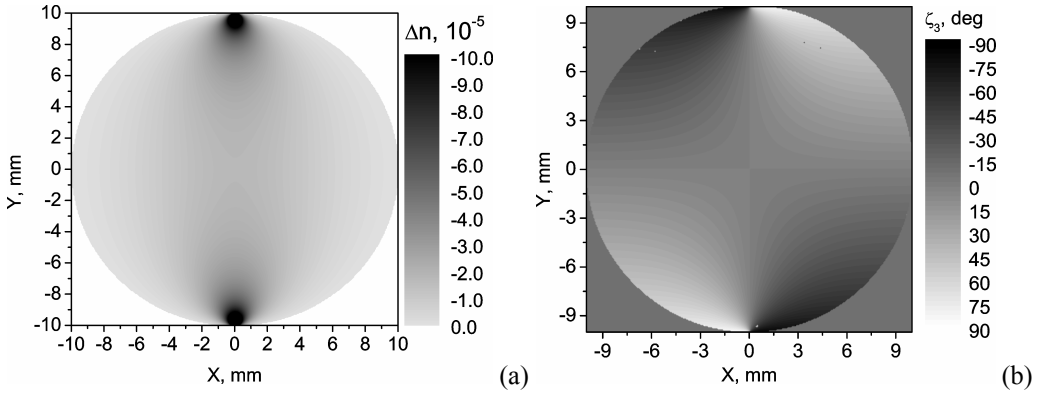

Fig. 1. Simulated distributions of birefringence and optical indicatrix rotation angle in $LiNbO_3$ induced in the XY plane by the uniaxial compressive force applied along the Y axis.

Now one can analyse the spatial distribution of the birefringence in the *XY* plane. For instance, we have $\sigma_6 = 0$ for the component σ_6 along the diameter $X = 0$ (i.e., the diameter parallel to the direction of loading force vector), while the components σ_1 and σ_2 are then equal to

$$\sigma_1 = \frac{P}{\pi dR}, \tag{10}$$

$$\sigma_2 = -\frac{2P}{\pi d}\left[\frac{2R}{R^2 - Y^2} - \frac{1}{2R}\right]. \tag{11}$$

The birefringence along this diameter is determined by the relation

$$\Delta n_{12} = -\frac{1}{2} n_0^3 (\pi_{11} - \pi_{12})(\sigma_1 - \sigma_2) = -n_0^3 (\pi_{11} - \pi_{12}) \frac{2RP}{\pi d\left(R^2 - Y^2\right)}, \tag{12}$$

while the angle of optical indicatrix rotation (see Eq. (8)) is equal to zero. Notice that the birefringence remains nonzero just at the origin of coordinates:

$$\Delta n_{12} = -n_0^3 (\pi_{11} - \pi_{12}) \frac{2P}{\pi dR}. \tag{13}$$

As a consequence, one can easily determine the difference of the coefficients $\pi_{11} - \pi_{12}$ using the nonlinear dependence of the birefringence on the *Y* coordinate obtained experimentally, along with Eq. (12).

Under the condition $Y = 0$, i.e. along the diameter perpendicular to the loading force vector, we have $\sigma_6 = 0$, though the other two components of the mechanical stress tensor remain nonzero:

$$\sigma_1 = -\frac{2P}{\pi d}\left[\frac{2RX^2}{\left(X^2 + R^2\right)^2} - \frac{1}{2R}\right], \tag{14}$$

$$\sigma_2 = -\frac{2P}{\pi d}\left[\frac{2R^3}{\left(X^2 + R^2\right)^2} - \frac{1}{2R}\right]. \tag{15}$$

In this case we have $\tan 2\zeta_3 = 0$, while the birefringence reads as

$$\Delta n_{12} = \frac{1}{2} n_0^3 (\pi_{11} - \pi_{12})(\sigma_1 - \sigma_2) = n_0^3 \frac{2P}{\pi d} (\pi_{11} - \pi_{12}) \frac{R(R^2 - X^2)}{(R^2 + X^2)^2}. \tag{16}$$

It is obvious that the difference of coefficients $\pi_{11} - \pi_{12}$ (and so the π_{66} coefficient) can be easy determined from Eq. (12) or Eq. (16), provided that the birefringence distributions respectively along the diameters parallel to the *X* or *Y* axes are known in advance. Moreover, one can determine the coefficients π_{11} and π_{12} separately using a standard interferometric technique, since the optical indicatrix orientation does not depend on the coordinates mentioned above (see [10]).

2.2. A disk perpendicular to X axis

When the disk is perpendicular to the *X* axis and the compressive force is applied along the *Z* axis, the nonzero components of the mechanical stress tensor are as follows:

$$\sigma_2 = -\frac{2P}{\pi d}\left[\frac{(R-Z)Y^2}{\left(Y^2+(R-Z)^2\right)^2}+\frac{(R+Z)Y^2}{\left(Y^2+(R+Z)^2\right)^2}-\frac{1}{2R}\right], \tag{17}$$

$$\sigma_3 = -\frac{2P}{\pi d}\left[\frac{(R-Z)^3}{\left(Y^2+(R-Z)^2\right)^2}+\frac{(R+Z)^3}{\left(Y^2+(R+Z)^2\right)^2}-\frac{1}{2R}\right], \tag{18}$$

$$\sigma_4 = \frac{2P}{\pi d}\left[\frac{(R-Z)^2 Y}{\left(Y^2+(R-Z)^2\right)^2}-\frac{(R+Z)^2 Y}{\left(Y^2+(R+Z)^2\right)^2}\right]. \tag{19}$$

In this case the equation for the optical indicatrix should be written as

$$\begin{aligned}&(B_1+\pi_{12}\sigma_2+\pi_{13}\sigma_3+\pi_{14}\sigma_4)X^2+(B_1+\pi_{11}\sigma_2+\pi_{13}\sigma_3-\pi_{14}\sigma_4)Y^2\\&+(B_3+\pi_{31}\sigma_2+\pi_{33}\sigma_3)Z^2+2(\pi_{44}\sigma_4-\pi_{41}\sigma_2)YZ=1\end{aligned}. \tag{20}$$

From Eq. (20) it follows that the birefringence increment and the angle of optical indicatrix rotation can be presented respectively as

$$\delta(\Delta n)_{23} \simeq \frac{1}{2}\left[n_o^3\left(\pi_{11}\sigma_2+\pi_{13}\sigma_3-\pi_{14}\sigma_4\right)-n_e^3\left(\pi_{31}\sigma_2+\pi_{33}\sigma_3\right)\right] \tag{21}$$

and

$$\tan 2\zeta_1 = \frac{2(\pi_{44}\sigma_4-\pi_{41}\sigma_2)}{B_1-B_3+(\pi_{11}-\pi_{31})\sigma_2+(\pi_{13}-\pi_{33})\sigma_3-\pi_{14}\sigma_4} \simeq \frac{\overline{n}^3}{\Delta n_{32}}(\pi_{44}\sigma_4-\pi_{41}\sigma_2) \tag{22}$$

with $\overline{n}=(n_3+n_2)/2$ and $\Delta n_{32}=n_3-n_2$.

Along the diameter Y = 0, one can rewrite Eqs. (21) and (22) with taking Eqs. (17)–(19) into consideration:

$$\sigma_2 = \frac{P}{\pi dR}, \tag{23}$$

$$\sigma_3 = -\frac{2P}{\pi d}\left[\frac{2R}{R^2-Z^2}-\frac{1}{2R}\right], \tag{24}$$

$$\sigma_4 = 0. \tag{25}$$

Then the birefringence increment is given by

$$\begin{aligned}\delta(\Delta n)_{23} &\simeq \frac{P}{2\pi dR}\left[n_o^3(\pi_{11}+\pi_{13}-\pi_{13}\frac{4R^2}{R^2-Z^2})-n_e^3(\pi_{31}+\pi_{33}-\pi_{33}\frac{4R^2}{R^2-Z^2})\right]\\&=\frac{P}{2\pi dR}\left[n_o^3(\pi_{11}+\pi_{13})-n_e^3(\pi_{31}+\pi_{33})+(n_e^3\pi_{33}-n_o^3\pi_{13})\frac{4R^2}{R^2-Z^2}\right]\end{aligned}. \tag{26}$$

At Z = 0, this relation looks like

$$\delta(\Delta n)_{23} = \frac{P}{2\pi dR}\left[n_o^3(\pi_{11}-3\pi_{13})-n_e^3(\pi_{31}-3\pi_{33})\right]. \tag{27}$$

Basing on Eq. (26) and the dependence simulated for the case of $LiNbO_3$ crystals (see Fig. 2), one can evaluate the combination $n_e^3\pi_{33}-n_o^3\pi_{13}$ of the piezooptic coefficients. Notice that our simulation has used the following values of the piezooptic coefficients: $\pi_{11}=-0.38\times10^{-12}\,\mathrm{m^2/N}$, $\pi_{13}=0.8\times10^{-12}\,\mathrm{m^2/N}$, $\pi_{31}=0.5\times10^{-12}\,\mathrm{m^2/N}$, and $\pi_{33}=0.2\times10^{-12}\,\mathrm{m^2/N}$ [13]. Then the

geometry Z = 0, Eq. (27) and the known difference $n_e^3\pi_{33} - n_o^3\pi_{13}$ would enable one to determine the combination of coefficients $n_o^3\pi_{11} - n_e^3\pi_{31}$.

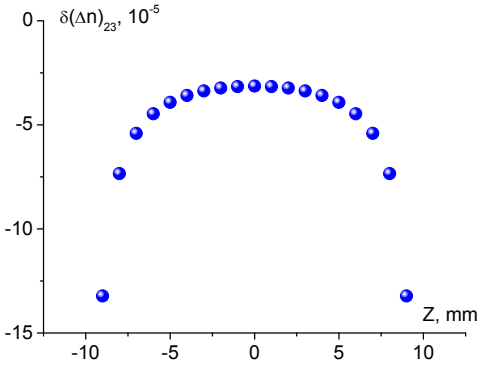

Fig. 2. Simulated dependence of birefringence increment on *Z* coordinate for the $LiNbO_3$ crystals.

Furthermore, one can find the coefficient π_{41} from the measured dependence of the optical indicatrix rotation angle (see Eq. (22)):

$$\tan 2\zeta_1 = \frac{\bar{n}^3}{\Delta n_{32}}\pi_{41}\frac{P}{\pi dR}. \tag{28}$$

It is also seen that the optical indicatrix rotation angle does not depend on the *Z* coordinate, being quite small (we have the value of 0.01 deg for the $LiNbO_3$ crystals, basing on the value $\pi_{41} = -0.88\times10^{-12}\,\mathrm{m}^2/\mathrm{N}$ [13]).

The stress tensor components needed to be accounted for along the diameter $Z = 0$ (i.e., the direction perpendicular to the applied force vector) are equal to

$$\sigma_2 = -\frac{2P}{\pi d}\left[\frac{2RY^2}{\left(Y^2+R^2\right)^2} - \frac{1}{2R}\right], \tag{29}$$

$$\sigma_3 = -\frac{2P}{\pi d}\left[\frac{2R^3}{\left(Y^2+R^2\right)^2} - \frac{1}{2R}\right], \tag{30}$$

$$\sigma_4 = 0. \tag{31}$$

Then the birefringence increment is given by the relation

$$\delta(\Delta n)_{23} \simeq -\frac{P}{\pi d}\left\{\left[\frac{2RY^2}{\left(Y^2+R^2\right)^2} - \frac{1}{2R}\right](n_o^3\pi_{11} - n_e^3\pi_{31}) + \left[\frac{2R^3}{\left(Y^2+R^2\right)^2} - \frac{1}{2R}\right](n_o^3\pi_{13} - n_e^3\pi_{33})\right\}. \tag{32}$$

Putting $Y = 0$ in Eq. (32), we arrive at

$$\delta(\Delta n)_{23} \simeq \frac{P}{2\pi dR}\left[n_o^3(\pi_{11} - 3\pi_{13}) - n_e^3(\pi_{31} - 3\pi_{33})\right]. \tag{33}$$

As seen from Fig. 3, one can easily determine the mentioned combination of the piezooptic coefficients (see Eq. (33)) using the dependence of the birefringence increment on the *Y* coordinate. It is interesting to notice that in this case the angle of the optical indicatrix rotation,

$$\tan 2\zeta_1 = -\frac{\overline{n}^3}{\Delta n_{32}}\pi_{41}\sigma_2 = \frac{\overline{n}^3}{\Delta n_{32}}\pi_{41}\frac{2P}{\pi d}\left[\frac{2RY^2}{\left(Y^2+R^2\right)^2}-\frac{1}{2R}\right], \tag{34}$$

does depend on the Y coordinate. The latter could serve as an additional tool while accurately determining the π_{41} coefficient. The corresponding dependence is shown in Fig. 4.

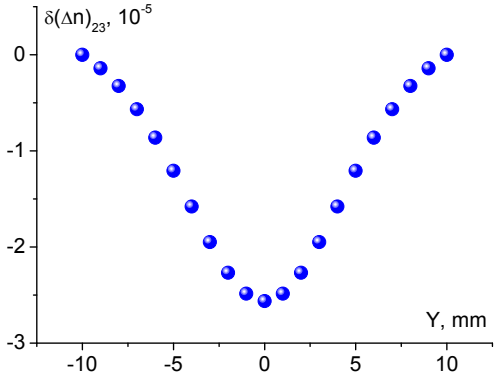

Fig. 3. Simulated dependence of birefringence increment on Y coordinate for the $LiNbO_3$ crystals.

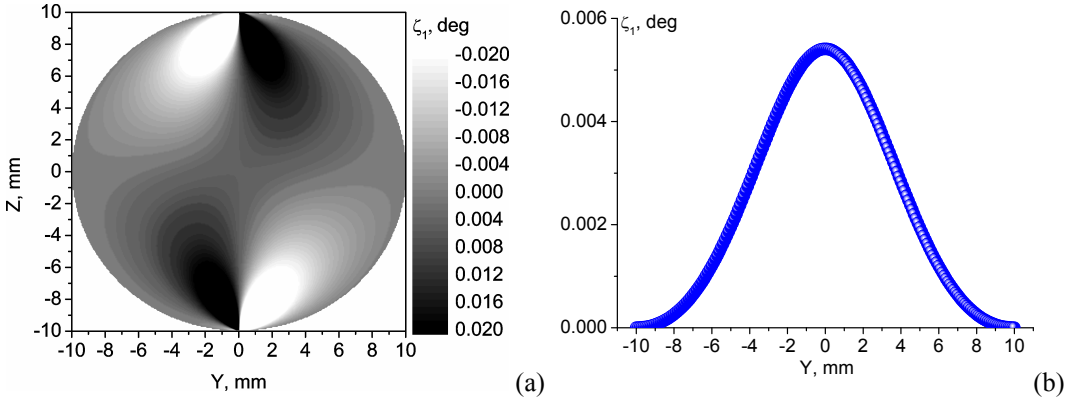

Fig. 4. Simulated map of optical indicatrix rotation angle (a) and its dependence on Y coordinate (b) for the $LiNbO_3$ crystals.

2.3. A disk perpendicular to Y axis

When the disk is perpendicular to the Y axis and the compressing force is applied along the X axis, the operating components of the mechanical stress are determined by the relations

$$\sigma_3 = -\frac{2P}{\pi d}\left[\frac{(R-X)Z^2}{\left(Z^2+(R-X)^2\right)^2}+\frac{(R+X)Z^2}{\left(Z^2+(R+X)^2\right)^2}-\frac{1}{2R}\right], \tag{35}$$

$$\sigma_1 = -\frac{2P}{\pi d}\left[\frac{(R-X)^3}{\left(Z^2+(R-X)^2\right)^2}+\frac{(R+X)^3}{\left(Z^2+(R+X)^2\right)^2}-\frac{1}{2R}\right], \tag{36}$$

$$\sigma_5 = \frac{2P}{\pi d}\left[\frac{(R-X)^2 Z}{\left(Z^2+(R-X)^2\right)^2}-\frac{(R+X)^2 Z}{\left(Z^2+(R+X)^2\right)^2}\right]. \tag{37}$$

The equation for the optical indicatrix can be written as

$$(B_1+\pi_{11}\sigma_1+\pi_{13}\sigma_3)X^2+(B_1+\pi_{12}\sigma_1+\pi_{13}\sigma_3)Y^2$$
$$+(B_3+\pi_{31}\sigma_1+\pi_{33}\sigma_3)Z^2+2\pi_{41}\sigma_1 YZ+2\pi_{44}\sigma_5 XZ+4\pi_{14}\sigma_6 XY=1 \quad (38)$$

Therefore the birefringence increment acquires is given by the formula

$$\delta(\Delta n)_{31}\simeq\frac{1}{2}\left[n_o^3\left(\pi_{11}\sigma_1+\pi_{13}\sigma_3\right)-n_e^3\left(\pi_{31}\sigma_1+\pi_{33}\sigma_3\right)\right], \quad (39)$$

while the angle of optical indicatrix rotation around the Y axis becomes

$$\tan 2\zeta_2=\frac{2\pi_{44}\sigma_5}{B_1-B_3+(\pi_{11}-\pi_{31})\sigma_1+(\pi_{13}-\pi_{33})\sigma_3}\simeq\pi_{44}\sigma_5\frac{\bar{n}^3}{\Delta n_{31}}$$
$$=\pi_{44}\frac{\bar{n}^3}{\Delta n_{31}}\frac{2P}{\pi d}\left[\frac{(R-X)^2 Z}{\left(Z^2+(R-X)^2\right)^2}-\frac{(R+X)^2 Z}{\left(Z^2+(R+X)^2\right)^2}\right] \quad (40)$$

The latter relation facilitates determination of the π_{44} parameter using measurements of the optical indicatrix rotation angle ($X\neq 0, Z\neq 0$). The corresponding map of the optical indicatrix rotation angle obtained due to computer simulations is presented in Fig. 5 (here we have used the value $\pi_{44}=2.25\times10^{-12}\,\mathrm{m^2/N}$ [13] for the piezooptic coefficient).

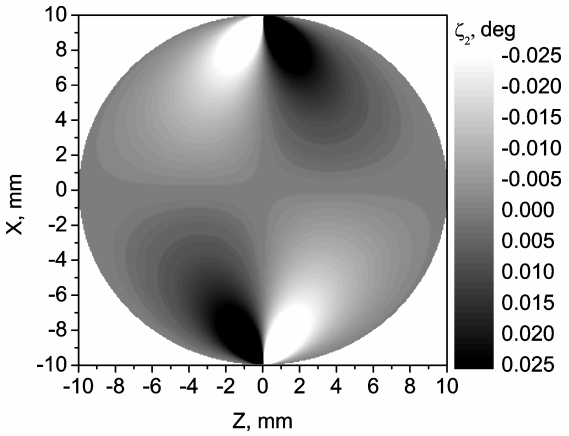

Fig. 5. Simulated map of angle of the optical indicatrix rotation around Y axis for the $LiNbO_3$ crystals.

The birefringence increment under the condition of $X=0$ is given by

$$\delta(\Delta n)_{31}\simeq-\frac{P}{\pi d}\left[\left[\frac{2R^3}{\left(Z^2+R^2\right)^2}-\frac{1}{2R}\right](n_o^3\pi_{11}-n_e^3\pi_{31})+\left[\frac{2RZ^2}{\left(Z^2+R^2\right)^2}-\frac{1}{2R}\right](n_o^3\pi_{13}-n_e^3\pi_{33})\right]. \quad (41)$$

In particular, we have

$$\delta(\Delta n)_{31}\simeq-\frac{P}{\pi d}\left[(n_o^3\pi_{11}-n_e^3\pi_{31})\left[\frac{2R}{R^2-X^2}-\frac{1}{2R}\right]+\frac{1}{2R}(n_e^3\pi_{33}-n_o^3\pi_{13})\right] \quad (42)$$

at $Z=0$. In other words, it is possible to determine the combination of the piezooptic coefficients after studying the dependence of the birefringence increment on the X or Z coordinates.

3. Experimental procedures and results

A sample of $LiNbO_3$ crystal used in our experiments was prepared in the shape of a disk, with its faces perpendicular to the Z axis. The sample had the radius 7.5 mm and the thickness 3 mm. The

YZ plane was accepted to be parallel to one of the symmetry mirror planes. A light of a He-Ne laser (the wavelength of $\lambda = 632.8$ nm) propagated along the *Z* axis.

The loading force ($P = 19.8$ N) was applied along the diameter of the disk parallel to the *Y* axis. We have used a polarimetric setup described earlier in the work [15]. While measuring the optical birefringence, we made the probing beam circularly polarized, thus avoiding unnecessary sensitivity of this beam to the orientation of optical indicatrix. Then the sample is described by a model of linear phase retarder, for which the dependence of the output intensity I on the analyzer azimuth α is expressed as

$$I = \frac{I_0}{2}\{1 + \sin\Delta\Gamma \sin[2(\alpha - \zeta_3)]\} = C_1 + C_2 \sin[2(\alpha - C_3)], \tag{43}$$

where ζ_3 is the orientation angle of the optical indicatrix and $\Delta\Gamma = 2\pi\Delta n_{12} d / \lambda$ the optical phase difference. After recording and filtering the image, azimuthal dependences of the intensity I were fitted by the sine function for every pixel of the image, with the fitting coefficients

$$C_1 = \frac{I_0}{2},\ C_2 = \frac{I_0}{2}\sin\Delta\Gamma,\ C_3 = \zeta_3. \tag{44}$$

It is evident that the optical phase difference $\Delta\Gamma$ is given by the coefficients C_1 and C_2:

$$\sin\Delta\Gamma = C_2 / C_1, \tag{45}$$

while the angular orientation of the intensity minimum is determined by the orientation of the principal axis ζ_3 of the optical indicatrix, together with the coefficient C_3. Hence, fitting of dependences of the light intensity measured behind the analyzer upon the azimuth for each pixel of the sample image should enable constructing 2D maps of the optical anisotropy parameters of that sample, i.e. the optical phase difference and the orientation of the optical indicatrix.

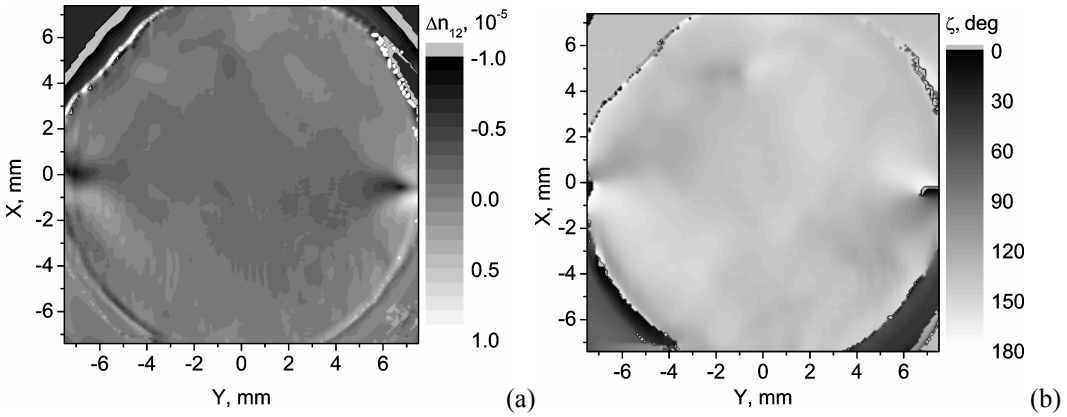

Fig. 6. *XY* maps of birefringence (a) and optical indicatrix rotation angle (b) induced in the $LiNbO_3$ crystals by the loading force 19.8 N (λ = 632.8 nm).

The maps of the induced optical birefringence and the optical indicatrix rotation angle measured experimentally are shown in Fig. 6. These maps are similar to the theoretical ones presented in Fig. 1. As a result, we have obtained the piezooptic coefficient $|\pi_{66}| = |\pi_{11} - \pi_{12}| = (0.20 \pm 0.01) \times 10^{-12}\,\mathrm{m}^2/\mathrm{N}$ using Eq. (12) and the corresponding birefringence distribution obtained experimentally along the *Y* axis (see Fig. 7). The error for the piezoptic coefficient does not exceed 6%. The piezooptic parameter obtained by us is smaller than that

reported in the work [13] ($\pi_{11} - \pi_{12} = -0.47 \times 10^{-12}\,\mathrm{m}^2/\mathrm{N}$), however the experimental error in the latter study has been essentially higher (~ 15%).

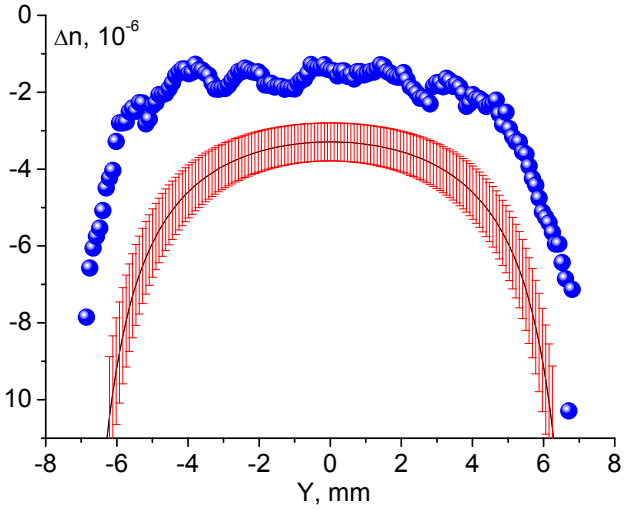

Fig. 7. Dependences of birefringence induced by the loading force 19.8 N in the $LiNbO_3$ crystals on *Y* coordinate: solid curve corresponds to calculations based on the piezooptic parameter $\pi_{11} - \pi_{12} = -0.47 \times 10^{-12}\,\mathrm{m}^2/\mathrm{N}$ [13], with the error bars displayed, and circles to our experimental results.

It is also worthwhile that the Poisson deformation does not affect the total phase difference measured in our case, since the initial birefringence along the *Z* direction is equal to zero. At the same time, the influence of the Poisson deformation on the total phase difference measured in the work [13] has been estimated following from the literature data on the elastic compliance coefficients. This should very likely give rise to some additional errors in determination of the piezooptic coefficients. Finally, we would also like to remind that the lithium niobate crystal is a well-known piezoelectric material where electrical polarization induced by the mechanical stresses can lead to additional changes in the birefringence, due to a so-called secondary electrooptic effect. In our experiments, the sample has been isolated and so this secondary effect indeed contributes to the total optical birefringence. On the other hand, as far as we know the electric conditions of the sample used in the work [13] have not been controlled at all.

4. Conclusion

In the present work we have suggested a precise enough experimental technique for determination of piezooptic coefficients. The technique is based on creating 2D distribution of mechanical stresses in a crystalline disk compressed along its diameter, which should be known in advance. Using a specific example of crystals that belong to the point symmetry group 3m, we have concentrated upon the differences of coefficients such as $\pi_{11} - \pi_{12}$, $n_o^3\pi_{11} - n_e^3\pi_{31}$, $n_e^3\pi_{33} - n_o^3\pi_{13}$, etc. These are the coefficients indicated as (A) in the matrix given by Eq. (2). We have proven theoretically that the above piezooptic parameters can be successfully determined after measuring the optical phase difference. In addition, the coefficients π_{44} and π_{41} can be calculated basing on the measurements of the optical indicatrix rotation angle. Finally, the technique suggested in this work has been verified on the example of the parameter $\pi_{11} - \pi_{12} = \pi_{66}$ for the $LiNbO_3$ crystals. We have shown that this piezoopic difference can be calculated with high enough accuracy. The mean absolute value of $\pi_{11} - \pi_{12} = \pi_{66}$ is equal to $(0.20 \pm 0.01) \times 10^{-12}\,\mathrm{m}^2/\mathrm{N}$, so that our experimental error does not exceed 6%.

References

1. Narasimhamurty T S, Photoelastic and electrooptic properties of crystals. New York: Plenum Press (1981).
2. Brewster D, 1815. Experiments on the depolarization of light as exhibited by various mineral, animal and vegetable bodies with a reference of the phenomena to the general principle of polarization. Phil. Trans. Roy. Soc. Lond. **105**: 29–53.
3. Brewster D, 1816. On the communication of the structure of doubly-refracting crystals to glass, murite of soda, flour spar, and other substances by mechanical compression and dilation. Phil. Trans. Roy. Soc. Lond. **106**: 156–178.
4. Vasylkiv Yu, Kvasnyuk O, Krupych O, Mys O, Maksymuk O and Vlokh R, 2009. Reconstruction of 3D stress fields basing on piezooptic experiment. Ukr. J. Phys. Opt. **10**: 22–37.
5. Mytsyk B, 2003. Methods for the studies of the piezo-optical effect in crystals and the analysis of experimental data. I. Methodology for the studies of piezo-optical effect. Ukr. J. Phys. Opt. **4**: 1–26.
6. Mytsyk B, 2003. Methods for the studies of piezooptic effect in crystals and analysis of the experimental data. II. Analysis of the experimental data. Ukr. J. Phys. Opt. **4**: 105–118.
7. Shaskolskaya M P, Acoustic crystals. Moscow: Nauka (1982).
8. Vasylkiv Yu, Savaryn V, Smaga I, Skab I and Vokh R, 2010. Determination of piezooptic coefficient π_{14} of $LiNbO_3$ crystals under torsion loading. Ukr. J. Phys. Opt. **11**: 156–164.
9. Skab I, Vasylkiv Yu, Savaryn V and Vlokh R, 2010. Relations for optical indicatrix parameters in the conditions of crystal torsion. Ukr. J. Phys. Opt. **11**: 193–240.
10. Krupych O, Savaryn V, Skab I and Vlokh R, 2011. Interferometric measurements of piezooptic coefficients by means of four-point bending method. Ukr. J. Phys. Opt. **12**: 150–159.
11. Skab I, Smaga I, Savaryn V, Vasylkiv Y and Vlokh R, 2011. Torsion method for measuring piezooptic coefficients. Cryst. Res. Techn. **46**: 23–36.
12. Frocht M M, Photoelasticity. London: J. Wiley and Sons (1965).
13. Mytsyk D G, Andrushchak A S, Demyanyshyn N, Kost' Ya P, Kityk A V, Mandracci P and Schranz W, 2009. Piezooptic coefficients of MgO-doped $LiNbO_3$ crystals. Appl. Opt. **48**: 1904–1911.
14. Weis R S and Gaylord T K, 1985. Lithium niobate: summary of physical properties and crystal structure. Appl. Phys. A. **37**: 191–203.
15. Skab I, Vasylkiv Y, Savaryn V and Vlokh R, 2011. Optical anisotropy induced by torsion stresses in $LiNbO_3$ crystals: appearance of an optical vortex. J. Opt. Soc. Amer. A. **28**: 633–640.

Vasylkiv Yu., Savaryn V., Smaga I., Krupych O., Skab I. and Vlokh R., 2011. Studies of piezooptic coefficients in $LiNbO_3$ crystals using a crystalline disk compressed along its diameter. Ukr.J.Phys.Opt. **12**: 180-190.

Анотація. *Ми запропонували новий, високоточний метод вимірювання п'єзооптичних коефіцієнтів, який базується на відомому 2D розподілі механічного напруження в кристалічному диску, стиснутому вздовж діаметра. Отримані відповідні теоретичні співвідношення, що описують п'єзооптичний ефект в кристалах, що належать до точкової групи симетрії 3т. Даний метод був експериментально перевірений з використанням кристалів $LiNbO_3$.*